

Exploring structural inhomogeneities in glasses during cavitation

Pinaki Chaudhuri^{1,2} and Jürgen Horbach¹

¹*Institut für Theoretische Physik II, Heinrich-Heine-Universität Düsseldorf, 40225 Düsseldorf, Germany*

²*The Institute of Mathematical Sciences, CIT Campus, Taramani, Chennai 600 113, India*

Using large-scale molecular dynamics simulations for a system of 10^6 particles, the response of a dense amorphous solid to the continuous expansion of its volume is investigated. We find that the spatially uniform glassy state becomes unstable via the formation of cavities, which eventually leads to failure. By scanning through a wide range of densities and temperatures, we determine the state points at which the instability occurs and thereby provide estimates of the co-existence density of the resultant glass phase. Evidence for long-lived, inhomogeneous configurations with a negative pressure is found, where the frozen-in glass structure contains spherical cavities or a network of void space. Furthermore, we demonstrate the occurrence of hysteretic effects when the cavitated solid is compressed to regain the dense glassy state. As a result, a new glass state is obtained, the pressure of which is different from the initial one due to small density inhomogeneities that are generated by the dilation-compression cycle.

PACS numbers:

INTRODUCTION

A common feature of the response of amorphous solids to a mechanical load is the formation of inhomogeneous structures that strongly affect the materials properties of these systems [1, 2]. Such structures can be associated with shear banding or (micro-)cavity formation and may lead to the initiation of crack formation or a strong brittleness [3–8]. Cavities are naturally formed when a liquid is expanded such that the two-phase region of gas-liquid coexistence is entered [9–14]. Similarly, the formation of cavities in dilated solids, during mechanical loading, can be considered as a process of phase separation and in fact, for model glass formers the metastable phase coexistence of a gas with a glass has been envisaged [15] and predicted [16]. However, a detailed microscopic insight into the formation of cavities in amorphous solids is lacking.

Different from the liquid-to-gas transition, one may expect that the phase-ordering kinetics of the glass-to-gas transition is affected by slowly relaxing (or even non-relaxing) glass domains, with a strong dependence on the history of these domains. Thus, the usual phase-ordering kinetics interferes with very slow relaxation processes that are associated with structural rearrangements in the system. On a theoretical basis, this interplay between a slow relaxation process and the phase separation process is only poorly understood. We note that, on a continuum level, earlier studies have considered the latter issue in the framework of a phenomenological model [17]. Recent work has explored such interplay via thermal quenches of a glass-forming liquid into the two-phase region [18, 19], investigating the resultant morphologies. In a silicate system, novel experimental techniques have been recently used to visualise the spatio-temporal evolution of such structures during similar thermal quenches leading to phase separation [20, 21], with the possibility that such studies can be extended to the glassy regimes.

In our work, molecular dynamics (MD) computer simulation are used to investigate a model glass former that is expanded towards a metastable miscibility gap where a glass is expected to coexist with a very low-density gas. During the expansion, the temperature is kept constant such that the system always remains in a glass state until the state point on the binodal is reached that separates the one-phase from the two-phase region (cf. Fig. 1). Beyond the binodal, we observe the formation of cavities, and we study their kinetics and analyze the dependence of various thermodynamic variables as well as the structure on time.

In the context of the phase-ordering kinetics of first-order phase transitions, different kinetic regimes can be identified that essentially depend on the distance of the considered thermodynamic state from the binodal of the transition. In the vicinity of the binodal, the formation of the new phase from its mother phase is an activated process that can be generally well described in the framework of classical nucleation theory (CNT) [22]. According to CNT, the nucleation rate, I , is given by $I = \kappa \exp \left[-\frac{\Delta F^*}{k_B T} \right]$, with κ a kinetic prefactor, k_B the Boltzmann constant, T the temperature, and ΔF^* the free energy barrier for the formation of a critical nucleus. Here, the free energy barrier ΔF^* is due to the competition between the free energy cost for the formation of an interface between the phases on the one hand and the free energy gain due to the formation of the new phase on the other hand. The kinetic prefactor κ depends essentially on the diffusion coefficient describing the mass transport in the mother phase. In most cases, the timescales for nucleation events, as described by CNT, are not accessible via molecular dynamics simulations. Further, in the context of gas-glass phase separation, the timescale for a cavity to emerge would also be impacted by the extremely long relaxation timescales of the glassy mother phase. However, if one moves farther away from the bin-

odal into the two-phase region, the barrier ΔF^* decreases and eventually the description in terms of CNT is not valid anymore. In this manner, one gradually approaches the regime of spinodal decomposition where fluctuations leading to the formation of the new phase spontaneously grow instead of being triggered by an activated process. An interesting question, in this context, is how such fluctuations and corresponding timescales are determined by the rate at which the volume expansion is done.

The goal of our MD simulation study is to understand how a spatially homogeneous amorphous solid in the two phase region becomes no longer stable, if subjected to continuous volume expansion. We observe an abrupt formation of a cavity accompanied by a homogeneous change of the density of the surrounding glass matrix. When keeping the total volume of the system constant, the kinetics of subsequent growth of the cavity is restricted due to extremely slow structural relaxation of the co-existing glassy material, although the system has a large negative pressure. As the volume expansion proceeds, the formation of cavities eventually leads to failure and disintegration of the amorphous solids. For each temperature, we mark the density at which cavitation occurs. At temperatures below a threshold, related to the line of mode coupling transition of the corresponding supercooled liquid, the cavitation density shows little temperature dependence. When we compress the cavitated solid to high densities, hysteretic effects are observed and the initial structure of the homogeneous amorphous solid is not entirely recovered. A new glass state is generated with small density inhomogeneities, remnant of the cavitation process during the expansion part of the cycle.

SETUP AND PROTOCOL

For our study, we carry out molecular dynamics simulations of a glass forming 80:20 binary AB Lennard-Jones (LJ) mixture, the details of which are given in Ref.[23]. The interinteraction potential is cutoff at a certain interparticle distance R_c and a smoothing function is used to ensure that both the potential and the forces continuously vanish at the cutoff distance [24]. All quantities are expressed in LJ units in which the unit of length is σ_{AA} , energy is expressed in the units of ε_{AA} , and the unit of time is $\sqrt{m\sigma_{AA}^2/\varepsilon_{AA}}$ where m is the mass of the particles. The cutoff range of the potential is chosen as $R_c = 2.5\sigma_{\alpha\beta}$, with $\alpha, \beta = A, B$ referring to the type of particles considered as a pair.

We prepare the amorphous solid by instantaneous quenches from the supercooled liquid. Most of our results are reported for a density of $\rho = 1.3$ where mechanically stable states, i.e. with positive bulk pressure, exist to very low temperatures. Quenches to target temperatures ($T = 0.5, 0.4, 0.3, 0.2, 0.1, 0.01$) are done from

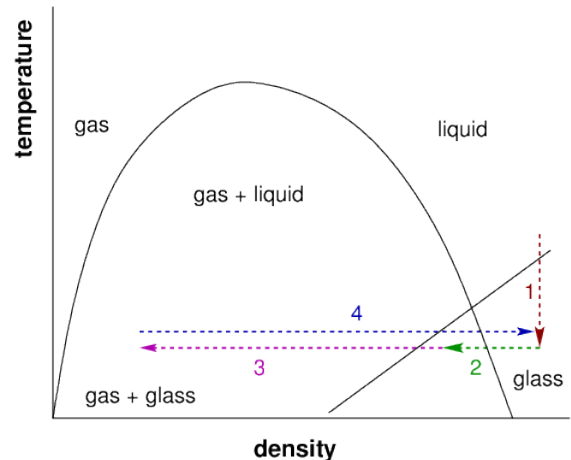


FIG. 1: Schematic diagram indicating the various paths traversed across the $T - \rho$ phase diagram in our numerical experiments. (1) - quench from supercooled liquid; (2) - expansion of amorphous solid until cavitation is observed; (3) - expansion of cavitated solid to explore low density states; (4) - compression of the cavitated solid back to initial high density.

equilibrated supercooled liquid states ($T = 0.66$) [26]. For some comparative studies, we also do simulations at $\rho = 1.2$ and $\rho = 1.4$. In those cases, the instantaneous quenches are done from $T = 0.44$ and $T = 0.945$, respectively, where the equilibrium diffusion constants are approximately similar to that measured at $T = 0.66$ for $\rho = 1.3$. Such quenches correspond to the path 1 marked in the schematic diagram shown in Fig. 1.

After the quench to the target temperature, the glass is aged for $t_w = 10^4$, before we begin our expansion experiments. Once aged, we carry out the following protocol for volume expansion. At every expansion step, we scale up the linear size of the cubic simulation box by a factor of $\Delta L = 1.001$ to obtain smaller densities. With the particle co-ordinates also getting similarly rescaled, this corresponds to an affine transformation of the system. Subsequently, we allow the system to relax over a time period of $\delta t = 10^3$, before the next expansion step is carried out. Some expansions are also done for smaller δt in order to compare the effects of the expansion rate. These expansion steps, at fixed temperatures, follow the paths 2 and 3, as marked on the schematic diagram (Fig. 1). We also report results from compression experiments, where the the linear size of the box is scaled by a factor of $\Delta L = 0.9990$, with intermediate $\delta t = 25$. This follows path 4 in Fig. 1, with the objective of returning back to the initial density from where the expansion of the solid was initially started. The expansion (or compression) protocol, described above, would correspond to ramp experiments. This is thus distinct from the protocol used in Ref. [8], where the solid was first expanded to certain strain amplitudes and thereafter the timescales for

a cavity to emerge were obtained.

Thermostatting at any temperature (T) is done by sampling velocities, at every 400 time steps, from the corresponding Maxwell-Boltzmann distribution. Here, we note that our expansion process is done under thermostatted conditions, unlike the micro-canonical NVE ensemble used in Ref. [8] (with E the total energy). Due to thermostating, there is no runaway heating as is the case in the NVE ensemble, due to the conservation of the total energy E .

The MD simulations are done for a system size of $N = 10^6$ particles, using the GPU-accelerated code HALMD [25]. For each state point that we have analysed, we do averages over $m = 10$ independent trajectories.

RESULTS

Onset of cavity

To monitor the thermodynamic state of the system during the expansion process (path 2 in Fig. 1), we measure the bulk pressure. With every step of expansion, the pressure drops as the particles are pushed apart. After each instantaneous expansion step, the pressure stabilises during the subsequent waiting time δt . As we decrease the density step by step, the pressure becomes negative implying the presence of internal tension. At some point during the expansion, the system can no longer sustain the built-up tension and the homogeneous system becomes unstable, with the occurrence of cavitation via a sudden increase in pressure [inset of Fig. 2(a)], similar to what has been observed in liquids [13]. This happens for all the configurations for the range of temperatures that we have studied. The variation of pressure with decreasing density and the onset of cavitation are shown in Fig. 2(a). We note here that the shape of the P vs. ρ isotherms are similar to those obtained by Sastry [16] for supercooled liquid states.

We record the density at which cavitation occurs for each of the m runs at each temperature T . The ensemble-averaged density for the onset of cavitation is marked on the phase diagram obtained by Testard *et al.* [18, 19]. We note that the *cavitation line* [see Fig. 2(b)] obtained by us lies to the left of the binodal line obtained in this earlier work. In the case of Testard *et al.* [18], the binodal line was obtained by measuring the density of the liquid/glass phase obtained during phase separation via thermal quenches. For us, the *cavitation line* marks the occurrence of the cavity within the time window of $\delta t = 10^3$ between each expansion step. We also further observe that, at low temperatures, i.e. below the extrapolated MCT-line [26], the density at which cavitation occurs does not differ much with T . However, as this MCT-line is crossed, thermal effects allow for the relaxation of local stresses built up during the expansion process, thus

increasingly delaying the emergence of cavities.

At the density at which cavitation occurs, we measure the partial structure factor corresponding to the correlations between particles of type A of the binary mixture, $S_{AA}(q)$, at the end of the time window δt (for a definition of $S_{AA}(q)$, see Ref. [27]). For all temperatures, we observe a similar low- q divergence in $S_{AA}(q)$ [see Fig. 2(c)], indicating the formation of a phase separated state [28].

We also check whether the density of cavitation depends upon the initial density of the quenched amorphous solid, from where the expansion process is started. Thus, at $T = 0.2$, we start the expansion from two other densities, viz. $\rho_0 = 1.2$ and $\rho_0 = 1.4$. Note that, for $\rho = 1.2$, at temperatures lower than $T = 0.2$, quenched amorphous states are unstable, i.e. they have negative pressure. Therefore, at this density, our dilation experiments are done for $T = 0.2$, such that we have stable homogeneous structures as initial states. We show in Fig. 2(d) that the onset of cavitation does not depend on ρ_0 . We have checked this to be the case for the ensemble of m initial states. Thus, the point of instability of the homogeneous amorphous solid does not seem to depend upon the amount of deformation undergone via the expansion protocol.

Density of co-existing glass

For properly marking out the boundaries of the phase diagram, knowing the density of the co-existing phases is required. Thus, we try to estimate the density of the glass (ρ_g) which is in co-existence with the low-density vapour phase. In order to measure that, we stop the expansion of the solid as soon as we identify that a cavity has formed in the system. We then proceed with the usual particle dynamics, holding the density constant at the cavitation density, and observe how the structure evolves with time.

In Fig. 3(a), for the glassy state at $T = 0.01$, we see that after the initial rapid increase of pressure, the rate of increase slows down and nearly saturates at long times. The evolution of the structure is also minimal, as can be seen from the $S_{AA}(q)$ at early and later times [see Fig. 3(b)]. The power-law divergence has an exponent of 3.74 which is close to Porod's law (corresponding to a smooth interface) [28]. To further illustrate the evolution of the structure, we compute the density iso-surfaces corresponding to $\rho = 0.2$ at several values of t [as marked in Fig. 3(a)] – this iso-surface encloses the low-density cavity. We see the emergence of the cavity as the jump in pressure initiates. When the pressure rapidly increases to release the local stresses, the cavity expands rapidly. At later times, the growth of the cavity slows down, when the time evolution of the pressure becomes very slow. We note that the pressure is still negative. While the system would like to release the residual tension to reach the non-negative co-existence pressure, the glassy dynamics of the

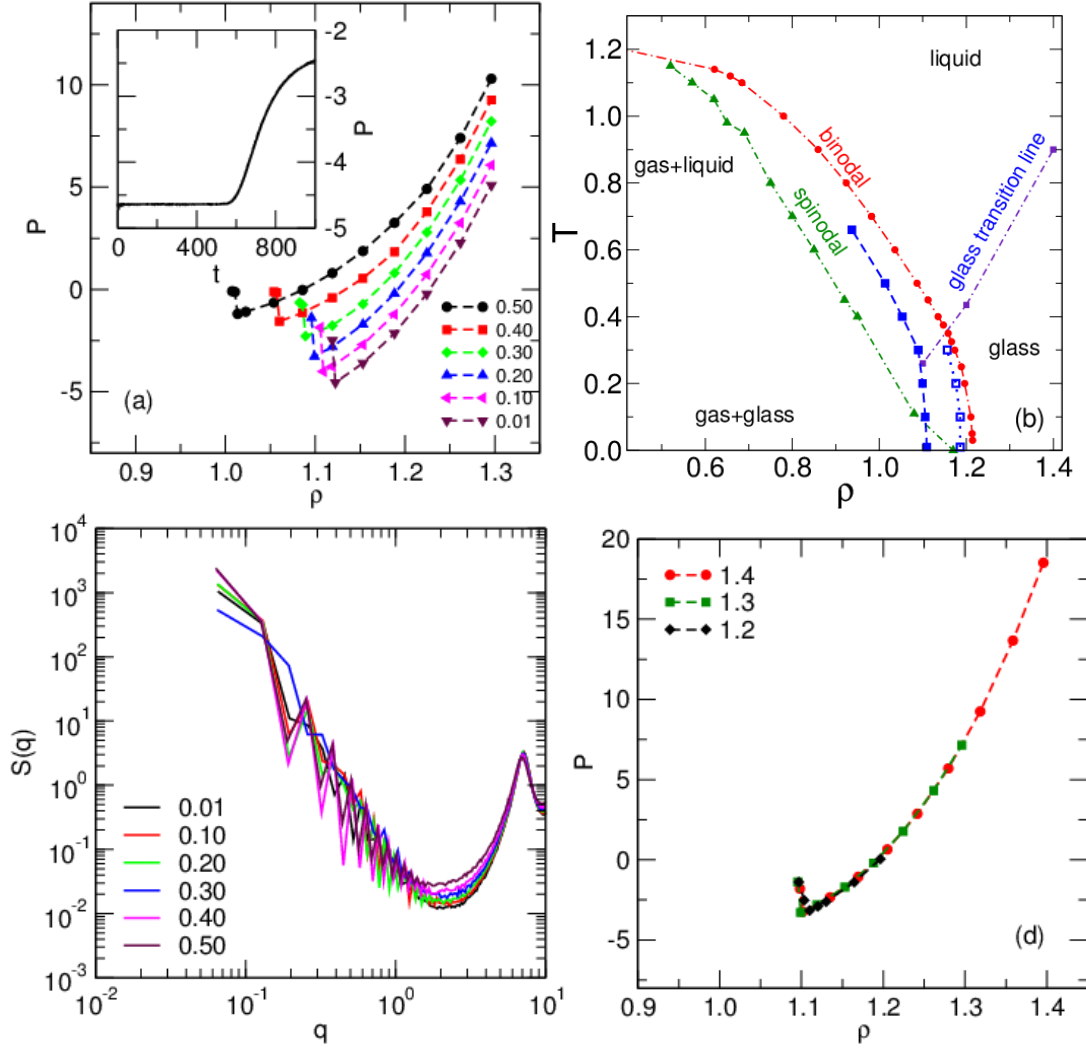


FIG. 2: (a) Evolution of pressure (P) with decreasing density ρ for the different temperatures $T = 0.01, 0.1, 0.2, 0.3, 0.4, 0.5$, with expansions starting from $\rho_0 = 1.3$. The inset shows the rapid increase in pressure when cavitation occurs inside the material; data is shown for $T = 0.01$. (b) For each temperature T , the density at which cavitation occurs is marked on the phase diagram by filled blue squares (the data is obtained from Ref. [19]). We also mark, using empty blue squares, the density of the amorphous solid which is in co-existence with the gas phase. (c) For different temperatures, the partial structure factor $S_{AA}(q)$ after cavitation is displayed. (d) P vs. ρ at $T = 0.2$ for states having initial densities $\rho_0 = 1.2, 1.3, 1.4$.

surrounding makes this process extremely slow. For comparison, we also show in Fig. 3(a) the time evolution of pressure during cavitation in a liquid state at $T = 0.66$. Firstly, the pressure values are much higher and unlike $T = 0.01$, the jump in pressure during the formation of cavity is smaller and also slower. Also, asymptotically, for the case of the liquid, the system is closer to a positive pressure state, unlike the glassy system.

As the cavity emerges, we start to measure the density of the amorphous solid which co-exists with the cavity. At every time of interest [marked in Fig. 3(a)], the cubic box is divided into smaller boxes having a linear dimension of 10 diameters. The local density is calculated in each small cube and the distribution is plotted. When phase separation occurs, we get a bimodal distribution;

ρ_g corresponds to the mean value of the distribution at high density. In the inset of Fig. 3(a), we show how ρ_g evolves with the time – the glassy matrix surrounding the cavity suddenly densifies following the emergence of a void. This densification process is also captured in $S_{AA}(q)$, as shown in the inset of Fig. 3(b); we see that, after cavitation, the location of the peak shifts to a larger wave-vector, indicating the emergence of a more dense solid.

For temperatures below the MCT line, we mark this asymptotic value of ρ_g in the phase diagram [Fig. 2(b) (using empty squares)]. The dependence on temperature is similar to our *cavitation line*. In accordance with Ref. [19], we also find that there is no low temperature re-entrant behaviour in ρ_g as suggested by Cardinaux *et*

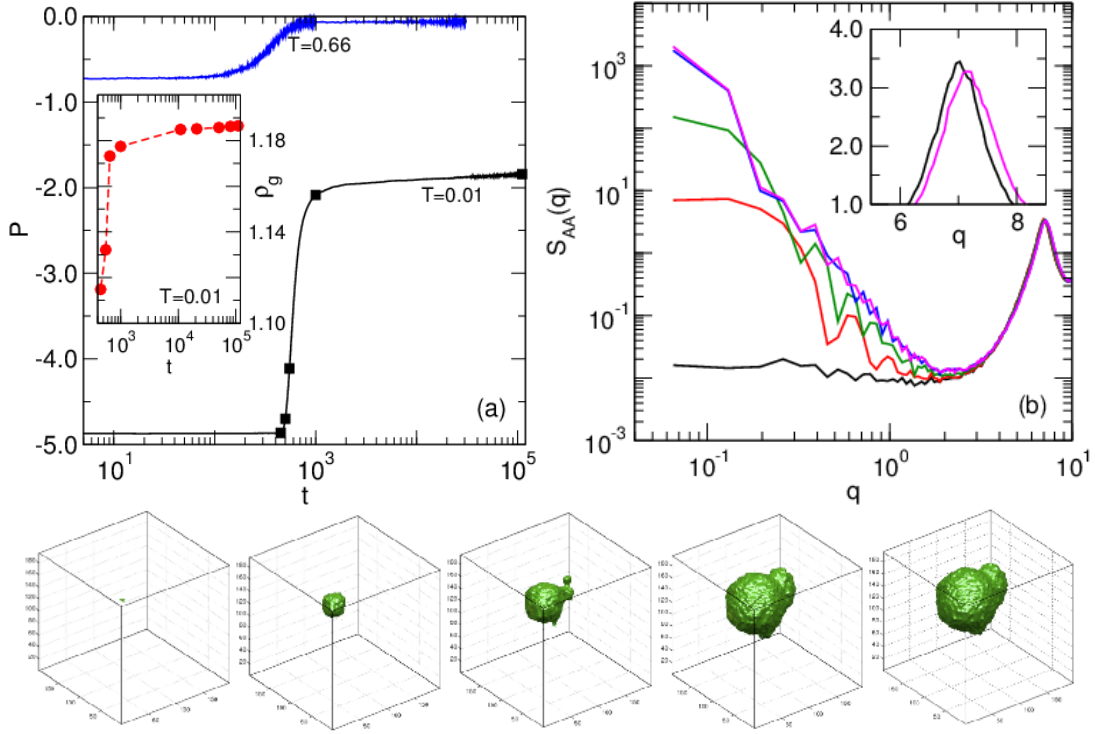


FIG. 3: **(Top)** (a) At $T = 0.01$, (in black) evolution of pressure with time, after cavitation, if the expansion is stopped (i.e. global density remains fixed). Also shown is the corresponding data for $T = 0.66$ (in blue). In the inset, the density of the amorphous solid co-existing with the low density phase inside the cavity is shown for $T = 0.01$. (b) Evolution of structure factor: $S_{AA}(q)$ measured at different times as marked in the main panel of (a) for $T = 0.01$. The inset shows that there is a shift in the location of the first sharp diffraction peak of $S_{AA}(q)$ between $t = 450$ and $t = 110000$, indicating a densification. **(Bottom)** Growth of cavity as a function of time: density plot showing evolution of the gas-solid interface at the above marked times.

al. [29]. We also note that our estimates of ρ_g are slightly smaller than those estimated in Ref. [19] – in our case, the existence of one or two cavities allows for easier estimation than compared to estimations from more complex structures as is the case for Testard *et al.* [19].

Exploring lower density states via expansion

In order to explore the process of large-scale failures in amorphous solids during dilation, we continue the expansion process beyond densities where cavities form (path 3 in Fig. 1). We wish to investigate how larger and more complex void spaces emerge as we continue the dilation. In order to expedite the exploration of a large range of densities within the simulational time scales, we resort to using a smaller δt , i.e. a smaller waiting time after each expansion step. Thus, we first check the effect of changing δt . As demonstrated in Fig. 4(a) for $T = 0.2$, the onset of cavitation is slightly delayed, i.e. with decreasing δt , it happens at lower densities ρ . Further, the jump in pressure at cavity formation is also rounded off. A smaller δt allows for less time for the structure to adjust to the expansion process, which delays the eventual

failure. This is consistent with the expectation that the time scale for cavitation becomes increasingly smaller as we move into the phase-coexistence region away from the binodal line. However, for all δt , once cavitation has occurred in each case, the pressure again increases with decreasing density as the system eventually tries to attain a stable state (corresponding to a positive pressure). Eventually, the P vs. ρ curves become nearly identical for the different δt we have explored, implying that the eventual stable states at smaller ρ do not depend on the rate of expansion.

For $\delta t = 25$, we travel to lower densities in the gas-glass coexistence region. We note that at densities around and less than $\rho = 0.469$, the pressure is nearly zero. In Fig. 4(b), we show the evolution of the structure, by measuring $S_{AA}(q)$, with decreasing ρ . To further visualise the evolution of the structure, we show the shape of the density field corresponding to the low-density phase that is in co-existence with the amorphous solid (see bottom panel of Fig. 4). We use the following colour code - the yellow iso-surface, corresponding to $\rho = 0.1$, faces the gas and the green iso-surface, corresponding to $\rho = 0.2$, faces the solid. Thus, initially, at high densities we have nearly spherical cavities emerging (cf. the snapshot for

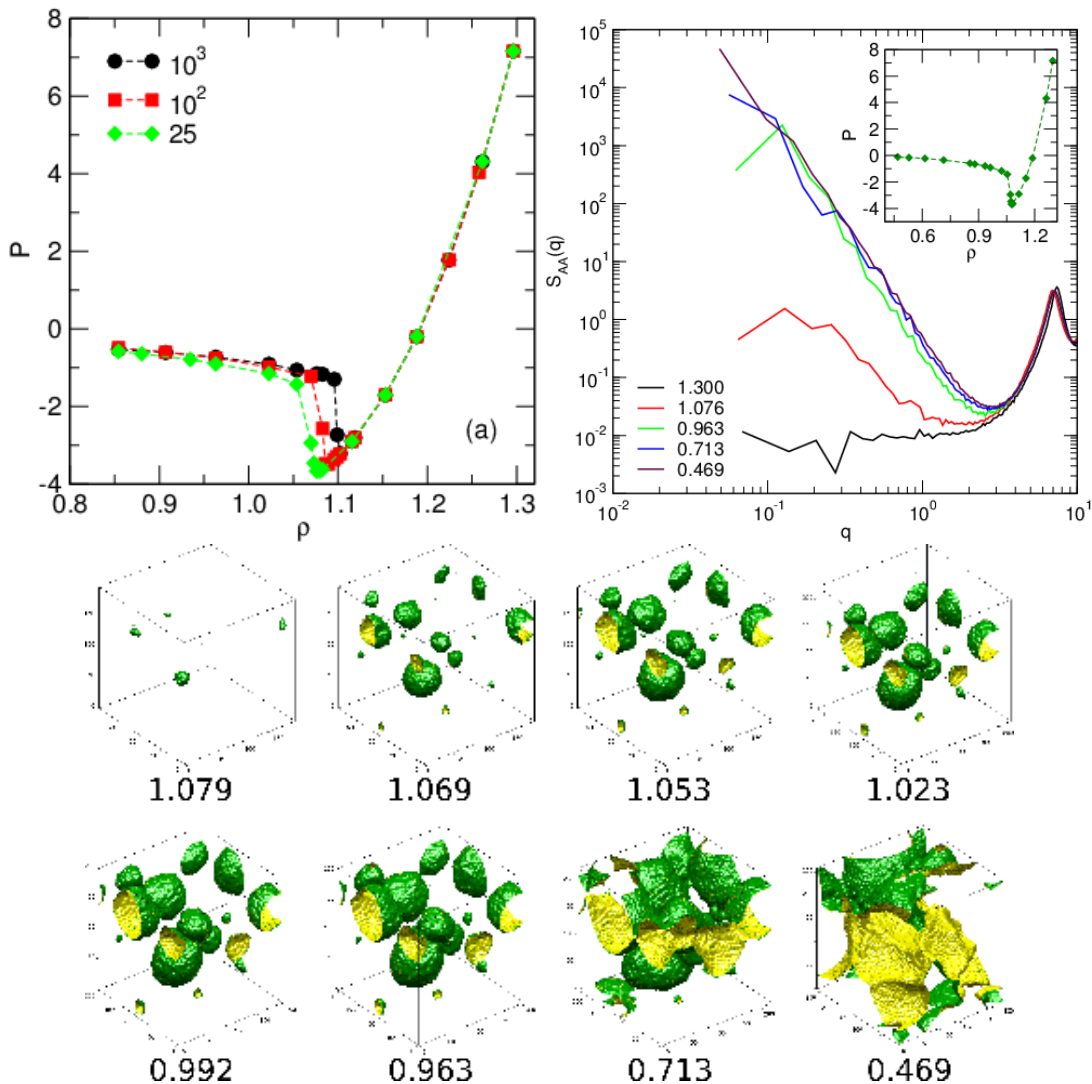


FIG. 4: *Continuing expansion*: **(Top)** $T = 0.2$: (left) evolution of pressure for different $\delta t = 1000$ (black), 100 (red), 25 (green). (Right) $S_{AA}(q)$ for $\rho = 1.3, 1.076, 0.963, 0.713, 0.469$. The inset shows the P vs. ρ data for the corresponding path across the phase diagram. **(Bottom)** Evolution of density field for $\delta t = 25$, with the green and yellow colours representing respectively the solid and gas sides of the interfaces.

$\rho = 1.069$). As the density is decreased, cavities merge and take more and more non-spherical shapes (cf. the snapshot for $\rho = 0.963$). Eventually, via the merger of these enclosed spaces, a interconnected structure emerges at lower densities (cf. the snapshot for $\rho = 0.469$). We note here that in experiments, the spatial percolation of the void space would correspond to the complete disintegration of the amorphous solid.

We have expanded the system further in order to estimate the density where the co-existence line is crossed in the low-density limit and a homogenous phase is observed, i.e. continuing along path 3 in Fig. 1. The sequence of states is illustrated using snapshots of particle configurations; see Fig. 5. As we explore smaller and smaller densities, eventually we obtain an amorphous cluster which is in co-existence with the gas (see, e.g., the

configuration at $\rho = 0.113$). We note that the cluster is not spherical in shape – one would expect that the forces due to surface tension would lead to smoothening out the surface of the cluster. However, because we are at low temperatures, the structural relaxation time scales are enormously large and therefore the interface does not relax further, leading to faceted surfaces. We have checked and found that even if we stop the expansion process and wait for long time scales, the shape of the cluster does not change due to the slow relaxation time scales. This is unlike the case for the liquid state where eventually a liquid droplet emerges to minimise the interfacial energy [22]. Finally, we note that even at densities as low as $\rho = 0.057$, the system remains phase-separated, i.e. the homogeneous phase corresponds to even lower densities, the exploration of which is beyond our current simula-

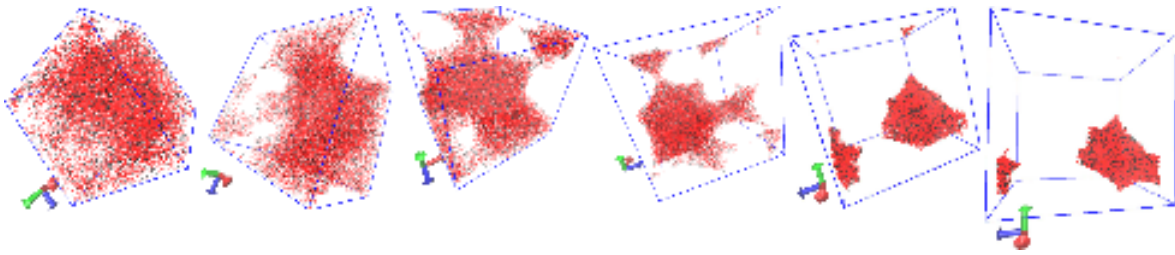


FIG. 5: Sequence of snapshots during volume expansion at $T = 0.2$. From left: $\rho = 0.963, 0.714, 0.529, 0.392, 0.113, 0.057$.

tional possibilities. This is consistent with the phase diagram obtained by Testard *et al.* [19], where we notice that the low temperature regime in the low density binodal is missing, possibly due to similar numerical difficulties.

Compressing the cavitated solid

Finally, we inquire how the material responds if the cavitated solid is compressed back towards the high density from where expansion was initiated. Starting from different low density states generated during the expansion, we carry out this compression process at fixed temperature (path 4 in Fig. 1). During the compression, we choose $\delta t = 25$. Data for the corresponding evolution of pressure with density is shown in Fig. 6(a) (using filled symbols). When the material is compressed, the pressure continually increases, as expected. We see that, apart from some initial regime, all these different initial low density states follow the same monotonic isotherm when the solid is compressed. Thus, if one considers the full expansion-compression cycle, there is a hysteretic effect which occurs via the cavitation process – the longer we wait before we begin the compression, the larger is the area under the loop.

In Fig. 6 (bottom), we visualise the low density regions inside the system, for the case where we compress the material from $\rho = 0.856$. With increasing density, the voids slowly shrink and eventually when the binodal is crossed the voids nearly disappear; see the density field for $\rho = 1.224$ in Fig. 6 (bottom). Going back to the isotherms shown in Fig. 6(a), we see that the variation of pressure with density becomes steeper beyond these densities. Once we reach the initial density ($\sim \rho = 1.3$) from where the expansion was started, we notice that the pressure is slightly higher than that of the undeformed quenched state. In fact, the partial structure factor [Fig. 6(b)] shows that the low- q behavior is different, implying that vestiges of the cavitation process (in the form of density inhomogeneities) have remained within the structure. The pressure thus increases to accommodate this structural change. Comparing two cases of compression beginning from $\rho = 1.069$ and $\rho = 0.856$, we find that the degree of mismatch in structures is more

pronounced for the lower initial density.

CONCLUSIONS

We have studied the process of phase separation in a model amorphous solid, via the continuous ramping up of its volume. We observed that, upon crossing the binodal line in the phase diagram, the spatially uniform glass becomes unstable, leading to the formation of cavities. For a given temperature, the density for cavitation depends upon the rate at which the expansion is done. This implies that the onset of phase separation is due to an interplay between the distance from the binodal and the time scale allowed for the structure to relax the increasing internal tension during successive dilation steps. For temperatures below the mode coupling transition line, thermal effects seem insignificant in determining the density for cavitation to occur, at a fixed expansion rate. However, above the line, thermal fluctuations allow faster relaxation time scales, thus delaying the onset of phase separation to increasingly smaller densities.

Similar to what has been reported in the context of crystal-to-glass transitions [30], we find the possibility of long-lived inhomogeneous glassy structures at negative pressures. This is different from gelation in systems with short-ranged attraction where the formation of a gel suppresses the onset of phase separation [31]. In the case of cavity formation in the glass, the extremely long relaxation time scales of the glassy matrix surrounding the cavities or the network of voids provide the long life-time of inhomogeneous structures. Such glassy time scales also lead to the formation of non-spherical amorphous clusters at very low densities, when the solid is further expanded. At some intermediate density, the void space percolates through the system, which would correspond to the failure of the solid in a real experiment.

We also explored the possibility of regaining the glassy state, if we compress the solid with cavities. We find that a single cycle of expansion and compression leads to hysteretic effects. There is a mismatch of structures at the initial density from where the cycle originated – the memory of the cavitation process is retained via the formation of a new inhomogeneous glassy state, with a

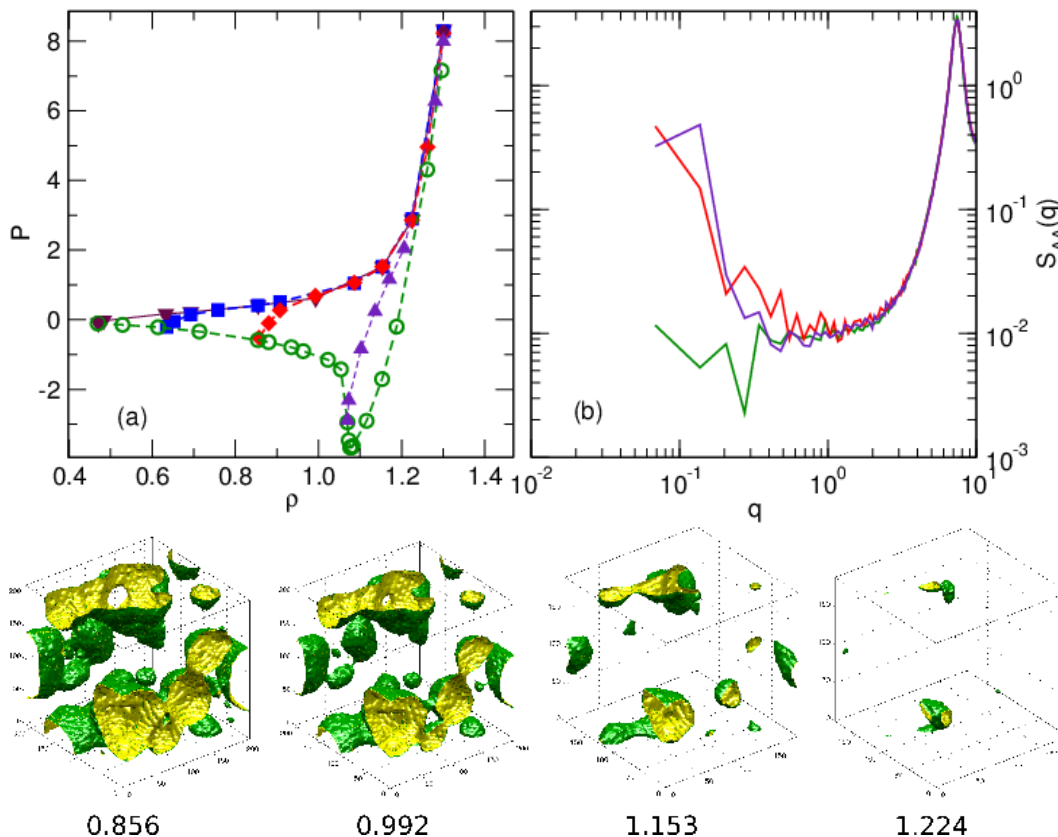


FIG. 6: **(Top)** (a) For $T = 0.2$ and $\delta t = 25$, evolution of the pressure with density (filled symbols) during compression, starting from different low densities (different colors). The corresponding P - ρ data for the expansion path is shown as empty symbols. (b) $S_{AA}(q)$ at $\rho = 1.30$ for the quenched amorphous state (in green) and the solid formed via compression starting from $\rho = 0.856$ (in red) and $\rho = 1.069$ (in purple). **(Bottom)** Density plots demonstrating how void spaces decrease in size as the material is compressed.

higher pressure, at the end of the cycle. As intermediate states during compression, we obtain porous structures which are mechanically stable. Thus, such expansion-compression paths are also possible routes to form amorphous porous solids.

Finally, we would like to note that one has to be careful when interpreting the onset of phase separation in the framework of classical nucleation theory. As we discussed earlier, the dynamic regime that is accessible by MD simulations is usually associated with the early stages of spinodal decomposition, in our case accompanied by the slow relaxation of the glass surrounding the cavity. A description in terms of CNT is, however, only sensible if the free energy barrier for the formation of a critical nucleus is much larger than the thermal energy, i.e. $\Delta F^* \gg k_B T$. In the work of Guan *et al.* [8], the measured free energy barriers for the cavity to form in a metallic glass are at most of the order of $10k_B T$. For such small barriers, cavity formation cannot be treated as an activated process, in contrast to the analysis by Guan *et al.* Further analysis is needed in understanding the cavitation in glasses, specially how barriers of phase separation interplay with the external stresses applied

during mechanical loading.

ACKNOWLEDGEMENTS

We thank the DFG research unit SPP 1594 (project HO 2231/8-1) for financial support. PC thanks the Starting Ramp Program within SPP 1594 for funding of GPU hardware. We also thank L. Berthier, M. Falk, W. Kob, and S. Sastry for useful discussions and N. Höft for the numerical analysis using HALMD.

-
- [1] C. A. Schuh, T. C. Hufnagel, and U. Ramamurty, *Acta Mater.* **55**, 4067 (2007).
 - [2] M. F. Ashby and A. L. Greer, *Scripta Mater.* **54**, 321 (2006).
 - [3] G. Wilde, J. H. Chen, C. B. Qu, S. Y. Fu, and F. Jiang, *Acta Mater.* **77**, 248 (2014).
 - [4] E. Bouchaud, D. Boivin, J. L. Pouchou, D. Bonamy, B. Poon, and G. Ravichandran, *EPL* **83**, 66006 (2008).

- [5] G. Wang, D. Q. Zhao, H. Y. Bai, M. X. Pan, A. L. Xia, B. S. Han, X. K. Xi, Y. Wu, and W. H. Wang, Phys. Rev. Lett. **98**, 235501 (2007).
- [6] P. Murali, T. F. Guo, Y. W. Zhang, R. Narasimhan, Y. Li, and H. J. Gao, Phys. Rev. Lett. **107**, 215501 (2011).
- [7] J.-Y. Suh, R. D. Conner, C. P. Kim, M. D. Demetriou, and W. L. Johnson, J. Mater. Res. **25**, 982 (2010).
- [8] P. Guan, S. Lu, M. J. B. Spector, P. K. Valavala, and M. L. Falk, Phys. Rev. Lett. **110**, 185502 (2013).
- [9] H. Maris and S. Balibar, Physics Today **53**, 29 (2007).
- [10] D. D. Joseph, J. Fluid Mech. **366**, 367 (1998).
- [11] D. W. Oxtoby, Acc. Chem. Res. **31**, 91 (1998).
- [12] T. Kinjo and M. Matsumoto, Fluid Phase Equil. **144** 343 (1998).
- [13] Q. An, G. Garrett, K. Samwer, Y. Liu, S. V. Zybin, S.-N. Luo, M. D. Demetriou, W. L. Johnson, and W. A. Goddard III, J. Phys. Chem. Lett. **2**, 1320 (2011).
- [14] V. G. Baidakov and K. S. Bobrov, J. Chem. Phys. **140**, 184506 (2014).
- [15] H. Tanaka, J. Phys.: Condens. Matter **12**, R207 (2000).
- [16] S. Sastry, Phys. Rev. Lett. **85**, 590 (2000).
- [17] K. Binder, H. L. Frisch, and J. Jäckle, J. Chem. Phys. **85**, 1505 (1986).
- [18] V. Testard, L. Berthier, and W. Kob, Phys. Rev. Lett. **106**, 125702 (2011).
- [19] V. Testard, L. Berthier, and W. Kob, J. Chem. Phys. **140**, 164502 (2014).
- [20] D. Bouttes, E. Guillard, E. Boller, D. Dalmas, and D. Vandembroucq, Phys. Rev. Lett. **112**, 245701 (2014).
- [21] D. Bouttes, O. Lambert, C. Claireaux, W. Woelfel, D. Dalmas, E. Guillard, P. Lhuissier, L. Salvo, E. Boller, and D. Vandembroucq, Acta Mater. **92** 233 (2015).
- [22] K. Binder, Rep. Prog. Phys. **50** 783 (1987).
- [23] W. Kob and H. C. Andersen, Phys. Rev. E **51**, 4626 (1995).
- [24] S. Toxvaerd, O. J. Heilmann, and J. C. Dyre, J. Chem. Phys. **136**, 224106 (2012).
- [25] P. H. Colberg and F. Höfling, Comp. Phys. Comm. **182**, 1120 (2011).
- [26] L. Berthier and G. Tarjus Phys. Rev. E **82**, 031502 (2010).
- [27] K. Binder and W. Kob, *Glassy Materials and Disordered Solids: An Introduction to Their Statistical Mechanics* (World Scientific, Singapore, 2011).
- [28] A. J. Bray, Adv. Phys. **43**, 357 (1994).
- [29] F. Cardinaux, T. Gibaud, A. Stradner, and P. Schurtenberger, Phys. Rev. Lett. **99**, 118301 (2007).
- [30] F. Sciortino, U. Essmann, H. E. Stanley, M. Hemmati, J. Shao, G. H. Wolf, and C. A. Angell, Phys. Rev. E **52**, 6484 (1995).
- [31] P. J. Lu, E. Zaccarelli, F. Ciulla, A. B. Schofield, F. Sciortino, and D. Weitz, Nature **453**, 499 (2008).